A1: Ferroelectric and Ferromagnetic Hysteresis Semiconductor Physics I - Laboratory

Hassan Tanveer - 3735258, Simon Briesenick - 3712933
Experiment conducted on: May 10th, 2021

I. Abstract

In this report, we investigate the ferroelectric and -magnetic properties of several samples. The hysteresis curves for magnetite are discussed and compared to literature. Additionally, the Verwey transition could be observed around $T_V = 115$K. For the ferroelectric analysis, we compared a single $PbZr_{1-x}Ti_xO_3$ thin film and a $10\times$[$BeFeO_3$-$BaTiO_3$] multilayer sample to a number of exemplary dynamic hysteresis measurements performed using a resistor and capacitor in parallel for different excitation frequencies f.

II. Theoretical Background

Magnetization and magnetic Susceptibility

When placed in magnetic fields, matter affects the effective magnetic field by a process called Polarization. In comparison to the vacuum case, the magnetic field vector $\mathbf{B}_{\text{matter}}$ will deviate from $\mathbf{B}$ in size (and for some materials even in direction). One speaks of **magnetization**. This is described by the equation

$$\mathbf{B}_{\text{matter}} = \mu\mathbf{B} = \mu\mu_0\mathbf{H} \tag{1}$$

The effect of the external magnetic field on the material is such that the direction of atomic, magnetic moments $\mathbf{p}_m$ is influenced by the field $\mathbf{B}$ in such a way, that a net Magnetization $\mathbf{M}$ builds up. The important point here is, that even though each one of the magnetic moments (either of nuclear spin or electronic spin and orbital motional nature) is affected by the external field $\mathbf{H}$, not all of them will assume their lower energy state position. In fact, thermal agitation and local fields are important influences opposing a uniform alignment of all the magnetic moments. However, in isotropic matter and for low magnetic field strengths the induced magnetic field will be aligned (or anti-aligned) to the external field. The magnetization vector is defined by

$$\mathbf{M} = 1/V \sum \mathbf{p}_m = \chi\mathbf{H}. \tag{2}$$

The magnetic susceptibility χ describes the strength and the alignment of the induced field $\mathbf{B}_{\text{ind}} = \mu_0\mathbf{M} = \mu_0\chi\mathbf{H}$ to the external field. One distinguishes the cases:

$|\chi| \ll 1$:

$$\chi = \begin{cases} \chi < 0, \text{for diamagnetic} \\ \chi > 0, \text{for paramagnetic materials} \end{cases} \tag{3}$$

and

$|\chi| \gg 1$:

$$\chi = \begin{cases} \chi < 0, \text{for antiferromagnetic} \\ \chi > 0, \text{for ferromagnetic materials} \end{cases} \tag{4}$$

The total field is thus

$$\mathbf{B} = \mu_0(1+\chi)\mathbf{H} \tag{5}$$

Comparison of eqn. (5) with eqn. (1) permits the identification of μ, known as the **relative permeability**, as

$$\mu = 1 + \chi. \tag{6}$$

Diamagnetism

Diamagnetic Materials are composed of atoms and molecules that do not have a permanent magnetic dipole moment $\mathbf{p}_m$. Instead, an external field induces dipole moments that tend to anti-align to it. In an inhomogeneous magnetic field, the substance is then pushed out of regions of larger magnetic field strength towards regions of weaker magnetic field strength. Diamagnetism is found in all materials and is only unobserved, when the stronger effects of paramagnetism or ferromagnetism are present. Diamagnetism can be classically be explained by treating the orbiting electron(s) using Maxwell's equations under an applied magnetic field. The idea behind the effect is that the change in magnetic moment of the electrons in the atoms causes a net magnetization that is oriented anti-parallel to the applied field. The susceptibility is calculated as

$$\chi = \frac{\mathbf{M}}{\mathbf{H}} \tag{7}$$

$$= -\frac{N\mu_0 Z e^2}{6m_e}\langle r^2\rangle_{\text{av}} \tag{8}$$

where N, Z and $\langle r\rangle_{\text{av}}$ are the atom number density, electron number per atom and the average radial distance of an electron from the atom, respectively. Langevin later recovered the same results using quantum mechanical theory.

Paramagnetism

In contrast to the diamagnetic case, atoms in paramagnetic materials already possess a permanent magnetic dipole moment $\mathbf{p}_m$. Such substances are drawn towards regions of higher magnetic field strength. For vanishing external fields,

the Magnetization of such a material also vanishes, since no direction is favorable. On average, the vector sum of the dipole moments adds up to zero for the previously mentioned reasons: $\mathbf{M} = 1/V \sum \mathbf{p}_m = \mathbf{0}$. Two theories are to be differentiated for paramagnetic materials. Firstly, the Langevin theory of paramagnetism which assumes that the magnetic dipoles of the material are only weakly coupled to each other (much weaker than thermal energy at most temperatuers). The dipole moments in a solid are then randomly oriented in the absence of an applied field $\mathbf{H}$. In an applied field however, the magnetization can be calculated using Boltzmann statistics. The (classical) result obtained by Langevin reads as

$$\mathbf{M} = N p_m \left[\coth\left(\frac{p_m H}{k_B T}\right) - \frac{k_B T}{p_m H} \right]. \tag{9}$$

The second square-bracketed term is also known as the Langevin function and was later modified by Brillouin to account for the spatial quantization of the magnetic moments:

$$\mathbf{M} = N g J \mu_B B_J(\alpha) \tag{10}$$

g, J and B_J are the Landé factor, the total angular momentum quantum number and the Brillouin function, respectively. The Brillouin function

$$B_J(\alpha) = \frac{2J+1}{2J} \coth\left(\frac{2J+1}{2J}\alpha\right) - \frac{1}{2J} \coth\left(\frac{\alpha}{2J}\right) \tag{11}$$

depends on $\alpha = J g \mu_B H / k_B T$ and equals the Langevin function in the limit $J \to \infty$. If $\alpha \ll 1$, the Brillouin function can be expanded in a Taylor series:

$$B_J(\alpha) = \frac{J+1}{3J}\alpha - \frac{[(J+1)^2 + J^2](J+1)}{90 J^3}\alpha^3 + \ldots \tag{12}$$

which after truncating up to the linear term in α gives the susceptibility as

$$\chi = \frac{N g^2 J(J+1)\mu_B^2}{3 k_B T} = \frac{C}{T} \tag{13}$$

and is known as Curie's law. Many paramagnetic substances do not obey Curie's law, but the more general Curie-Weiss law above a certain critical temperature θ

$$\chi = \frac{C}{T - \theta}. \tag{14}$$

Weiss pointed out the significance of θ in this equation: the material behaves magnetically as if there were some additional field (which he called the molecular field), $\gamma\mathbf{M}$, that aids the true field $\mathbf{H}$. Indeed, letting $\theta = \gamma C$, one may write for the magnetization

$$\mathbf{M} = \frac{C(\mathbf{H} + \gamma \mathbf{M})}{T}. \tag{15}$$

This is a contradiction to the Langevin theory of paramagnetism, where the elementary magnet is supposed to not have an influence on its neighbours. As $T \to \theta$, there is a divergence in the susceptibility, which corresponds to the phase transition of the material to the spontaneously ordered phase, discussed next. The second theory for paramagnetic materials is named after Pauli, where the susceptibility is found to be independent of temperature in certain conductors. Pauli

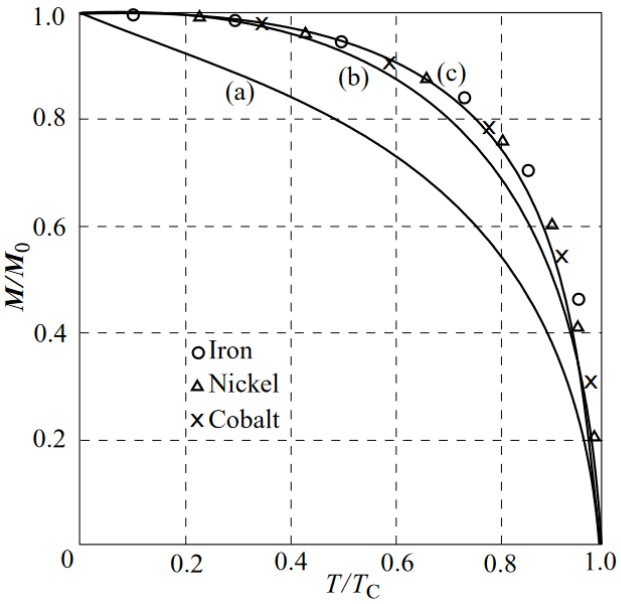

Fig. 1: Relative Magnetization of Fe, Co and Ni as a function of the relative temperature. (a) corresponds to the classical result given by the Langevin theory, (b) and (c) are the results when the Brillouin function with $J = 1$ or $J = 1/2$, respectively, is used. From [1].

paramagnetism for metals that fit the free-electron model gives for the susceptibility

$$\chi = \frac{\mu_0 \mu_B^2 (N/V)}{E_F}. \tag{16}$$

Ferromagnetism

Led by his discovery of the molecular field in paramagnets, Weiss assumed further that a molecular field must also be present below temperatures θ that correspond to the phase transition from the paramagnetic to the ferromagnetic phase. To explain the magnetic behaviour of ferromagnets, this molecular field must be strong enough to spontaneously magnetize the material. Indeed, under the assumption the magnetic field is now entirely supplied by this molecular field, $\mathbf{H} = \mathbf{0}$, stable solutions for the magnetization exist provided the temperature is lower than the Curie temperature $\theta = T_C$. The magnetization value M of a material in the absence of an applied field can be given as

$$\frac{M}{M_0} = \tanh \frac{M/M_0}{T/\theta}, \tag{17}$$

where M_0 is the value at absolute zero. This equation implies that for all temperatures below θ, the intensity of magnetization has a definite value even when there is no applied field present. The origin of the molecular field was not explained by Weiss, who proposed his phenomenological model of ferromagnetism in 1907 [2]. Instead, it was Heisenberg in 1928 [3], who showed that a quantum mechanical treatment of the multibody problem could explain the origin of the molecular field. Indeed, in quantum theory, the energy of interaction between two neighbouring atoms has an additional contribution, known as the exchange integral which tends to orient the electron

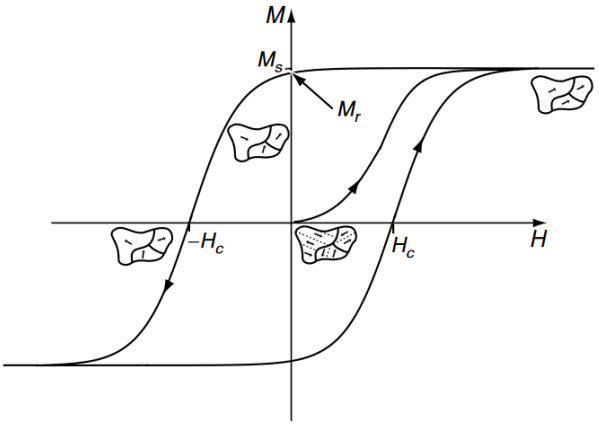

Fig. 2: A typical ferromagnetic or ferrimagnetic hysteresis loop. From [5], p. 8

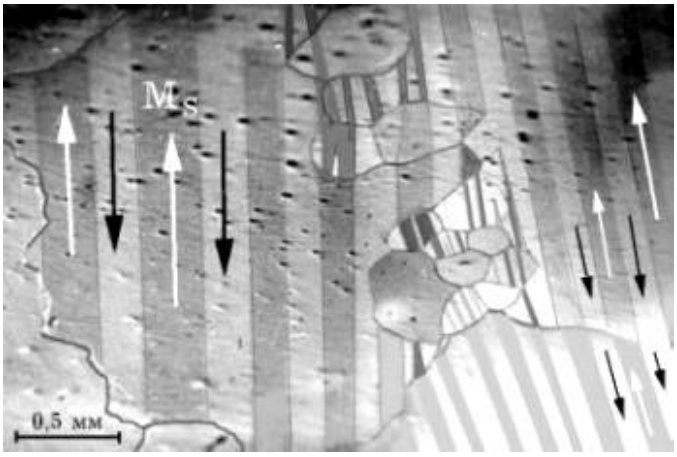

Fig. 3: Domain pattern in Fe + 3% Si. From [6].

spins parallel to each other. Further insight into the quantum mechanical treatment of the exchange interaction can be found in [3] and [4]. Weiss also explained why a piece of ferromagnetic material is apparently unmagnetized at room temperature: all parts of the material are magnetized to saturation, but different parts are magnetized in different directions (mostly along the easy axes) so that the overall effect is zero. Even though a perfect alignment of all of the magnetic moments would minimize the exchange energy, it also maximizes the magnetostatic energy, which is important especially close to the surface of the material. This is the concept known as Weiss domains. The shape and size of the domains are determined largely by magnetocrystalline and magnetostrictive energies. Each part with uniform magnetization makes up one domain and is separated from neighbouring domains by walls across which the magnetization direction changes drastically. When the unmagnetized material is now placed in an applied field $\mathbf{H}$, those domains, whose magnetizations already make an energetically favourable angle with the applied field will start to grow in size. Neighbouring domains will experience a sudden change in direction of magnetization until the entire material is magnetized uniformly (in the hysteresis curve this would be the knee of the magnetization). Subsequently, after increasing the applied field even further, the magnetization vector of the now uniformly magnetized material is slowly turned so as to align it with the applied field. A typical magnetization curve is shown in Fig. 2. After reaching saturation M_S, decreasing the applied field back to zero will not reproduce the same virgin state as before placing the material in the magnetic field. There will, however, be some remnant magnetization M_r, albeit lower that the value at saturation. The physical reason behind the decrease in magnetization is due to partial reorientation of domains, especially at the boundaries of the material due to the previously mentioned magnetostatic energy. To completely demagnetize the material again, an oppositely oriented applied field $-H_C$ needs to be reached, called the coercive field. Upon closer examination of the hysteresis curve, the flipping of individual domains can be observed. Indeed, this is called the Barkhausen effect; the magnetization curve takes discontinuous steps as $\mathbf{H}$ is varied. These step sizes can be used to give a measure for the volume of a single domain. The domains can also be observed on the surface of demagnetized ferromagnets (for example by placing small colloidal magnetic particles on it), see Fig. 3.

Antiferromagnetism and Ferrimagnetism

In antiferromagnetic and ferrimagnetic materials, two interpenetrating sublattices of magnetic ions (A and B) determine the magnetic behaviour. In antiferromagnetic materials, the individual magnetization of one species of ions, $\mathbf{M_A}$ is equal and opposite to the magnetization of the second species that composes the other sublattice, $\mathbf{M_B}$ in the absence of an applied field. Before the publication of Néel's paper in 1952 [7], it was empirically known, that the susceptibility in antiferromagnets above the (later termed) Néel temperature T_N, obeys the Curie-Weiss law, but with a negative value of θ, i.e.

$$\chi = \frac{C}{T-(-\theta)}. \tag{18}$$

A negative value for θ would however imply that the molecular field, $\theta = \gamma M$ would be negative in the sense that it tends the magnetic moments to anti-align. The total fields acting on each sublattice are [5]

$$\mathbf{H_A^t} = n_{AA}\mathbf{M_A} + n_{AB}\mathbf{M_B} + \mathbf{H} \tag{19}$$

$$\mathbf{H_B^t} = n_{BA}\mathbf{M_A} + n_{BB}\mathbf{M_B} + \mathbf{H} \tag{20}$$

where $n_{AA} = n_{BB}$ and $n_{AB} = n_{BA}$ are coupling constants and $\mathbf{H}$ being an externally supplied field. Below the Néel point and without an external field, the spontaneous magnetization of each sublattice is represented by the Brillouin function

$$M_i = \pm M_0 B_J(\alpha) \tag{21}$$

where $i = A, B$ and α as defined above for each sublattice and with the respective sign for M_0. Each sublattice spontaneously magnetizes below the Néel point. Connecting eqns. 19 and 20 to the condition that above the Néel point, the material behaves like a paramagnet, serves to solve for T_N in terms of the coupling constants as

$$T_N = 2C(n_{AA} - n_{AB}) \tag{22}$$

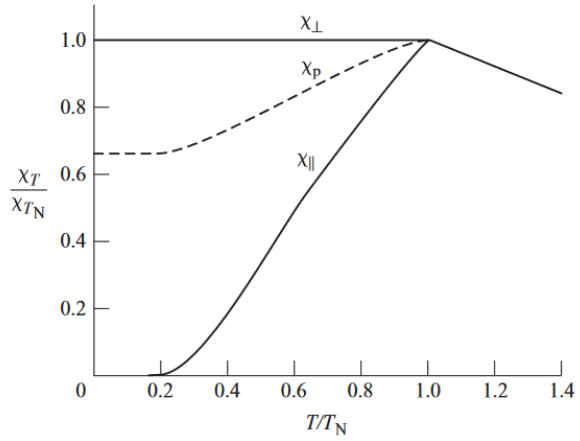

Fig. 4: Susceptibility in antiferromagnetic materials. The two dashed line is due to a polycrystalline or powdered sample and shows a mixture of the two contributions. Above T_{N}, the material behaves paramagnetically. From [4], p. 107.

where C is the Curie constant from eqn. 18. In applied fields, the net magnetization generally differs from 0, since the magnetization direction of the sublattice is now energetically biased, in the sense that the preferred magnetization direction now lies along the applied field axis. The susceptibility in an antiferromagnet is a tensor, owing to magnetic anisotropy. The two limiting cases for the field direction $\mathbf{H}$ are parallel and perpendicular to the sublattice magnetization axes. For the parallel susceptibility one obtains [4]

$$\chi_{\parallel} = \frac{2Np_m^2 B_J'(\alpha)}{2k_B T + Np_m^2 \gamma B_J'(\alpha)} \tag{23}$$

where B_J' is the derivative of the the Brillouin function with respect to α. The perpendicular susceptibility is [4]

$$\chi_{\perp} = \frac{1}{\gamma} \tag{24}$$

which is a constant. For a general direction, the susceptibility is a linear combination of the two depending on the relative angle of the field. A typical temperature dependence for the susceptibility is shown in Fig. 4. Evidence for the sublattice magnetic ordering of antiferromagnets was first gathered in 1949 by Shull and Smart [8] using Neutron diffraction. The origin of the antiparallel molecular field alignment is called superexchange and more detail can be found in [4].

The magnetic structure of ferrimagnets is similar to antiferromagnets. The sublattices are however not structurally identical. The magnetizations in eqns. 19 and 20 can not be simplified in this case by the assumption that $n_{AA} = n_{BB}$. However, each sublattice can still be accurately described by the Brillouin functions as given in eqn. 11 as long as the temperature is below the ferrimagnetic Néel temperature T_c at which point the two magnetization components collapse to zero. Ferrimagnets show a similar hysteresis curve to ferromagnets (see Fig. 2, although the saturation magnetization is usually much lower. Since the magnetization components $\mathbf{M_{A,B}}$ do not need to have the same temperature dependence, under certain conditions the sublattice magnetizations can be made to exactly cancel each other out at an intermediate temperature T_{comp}.

Ferroelectricity, Antiferroelectricity

Ferroelectric behavior was first described in 1921 in single crystal Rochelle salts [9] and was subsequently also investigated in polycrystalline ceramics as Barium titanate, $BaTiO_3$. The name *ferroelectricity* is a bit of a misnomer, since a ferroelectric material does in general not contain iron, as the name would suggest. However, the behaviour of ferroelectrics in electric fields was found to be analogous to ferromagnetics in magnetic fields, which were discovered earlier. The governing principle behind ferroelectricity is however due to an asymmetry in charge (either ionic or electronic) and not in electron spin (as in ferromagnets). Conceptually, ferroelectric behaviour shows many similarities to ferromagnetism. A ferroelectric is a material with a spontaneous electrical polarization that can be switched with an externally supplied electric field. The switching process is associated with a hysteresis curve in a P-E plot. The macroscopic polarization of a ferroelectricum can vanish by the presence of domains. The spontaneous polarization magnitude will also vanish at a certain critical temperature T_C (also termed Curie temperature) beyond which the material behaves paraelectrically. This phase transition from the ferroelectric to the paraelectric phase as a function of temperature is often accompanied with a discontinuous jump in the polarization of the investigated material. The relation between antiferroelectricity and ferroelectricity can be understood in analogy to antiferromagnetism and ferromagnetism.

Pyro and Piezoelectricity

Ferroelectric materials are in fact a subsection of the greater set of materials, termed pyroelectric. Pyroelectricity describes the ability of materials to generate a temporary voltage upon heating or cooling, which is due to the temperature dependence of the magnitude of the spontaneous polarization of a pyroelectric crystal. Piezoelectricity, discovered in 1880 by the Curie brothers, describes the generation of electric charge that is proportional to mechanical stress. The converse piezoelectric effect is the reversible measurement of mechanical stress upon applying a voltage across the material. For symmetry reasons, a ferroelectric crystal is always also piezoelectric.

III. Experimental Setup

Ferromagnetic Analysis

The Vibrating Sample Magnetometer (VSM) by Quantum Design was used for recording the magnetic data. The magnetometers basic functionality is described briefly in the following. The sample is mounted on a sample rod and is driven sinusoidally in a variable, external magnetic field generated by an outer, secondary coil. A pickup coil measures the changing magnetic flux by Faraday's law. Indeed, a (varying) voltage is induced in the pickup coil via [10]

$$V_{\mathrm{coil}} = \frac{d\Phi}{dt}. \tag{25}$$

which in term of the material parameter m (DC magnetic moment) can be solved to be

$$V_{\text{coil}} \propto fmA \sin(ft) \tag{26}$$

where A is the amplitude of vibration and f the oscillation frequency. The driving frequency of the sample holder is designed to operate at 40 Hz.

Ferroelectric Analysis

In order to measure field-dependent polarization $\mathbf{P}(U)$-loops, the current response I to an external voltage U is recorded across a sample capacitor structure with area A. For the polarization it follows that

$$\mathbf{P} = \frac{Q}{A} = \frac{\int I dt}{A} \tag{27}$$

where Q is the generated charge on the capacitor. The aixACT aixPlorer Software was used to implement the measurements. The measurements were performed as dynamic hysteresis measurements (DHMs) which are characterized by four triangular excitation pulses over a time period of $1/f$, the first one being the prepolarizing pulse. DHM are typically preferred to static hysteresis measurements, since leakage currents and resistance breakdown is to be avoided, which are much more important factors in SHMs.

IV. Material Information

Magnetite

Technologically the most important ferrimagnets are the materials known as ferrites. Magnetite belongs to the subgroup of cubic ferrites - materials that crystallize in the spinel or inverse spinel structure, named after the mineral spinel $MgAl_2O_3$. The general chemical formula of cubic ferrites is $MO \cdot Fe_2O_3$, where M is a divalent ion such as Mn^{2+} or Fe^{2+} [4]. Magnetite is found in the inverse spinel structure, where oxygen anions are packed in a fcc arrangement with tetrahedral and octahedral interstitial sites. One-eight of the tetrahedral sites and half of the octahedral spaces are occupied by Fe^{3+} and $Fe^{2+/3+}$A and B cations. Hence, for every tetrahedral iron ion, a pair of of octahedrally coordinated ($Fe^{2+/3+}$) ions in the adjacent layer can be found. The sites form coplanar layers perpendicular to the $[1\,1\,1]$ direction and the quantum mechanical superexchange anti-aligns the two layer magnetizations, as discussed above. A schematic of the crystal structure is shown in Fig. 5. Furthermore, magnetite has a Néel temperature of $T_{\text{N}} = 860\text{K}$.

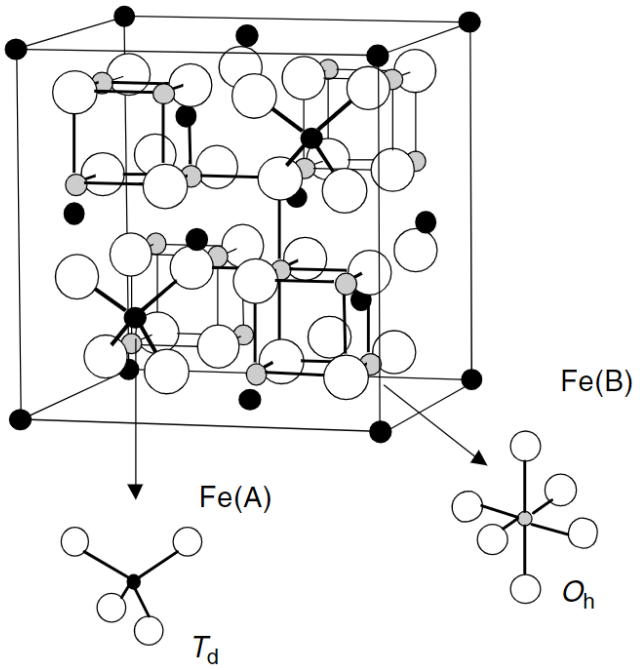

Fig. 5: Crystal structure of spinel Fe_3O_4. The large, white circles represent oxygen ions, the black and grey ones denote A and B sites, respectively. From [18], p. R148.

Structural Phase Changes in $BaTiO_3$

Barium titanate is is a common ferroelectric insulator (However, it can be transformed into a semiconductor with appropiate doping) that has a perovskite structure. Solid $BaTiO_3$ can exist in five phases which are (from high to low temperature): hexagonal, cubic, tetragonal, orthorhombic and rhombohedral. All phases except the cubic one exhibit ferroelectric behaviour. The charge asymmetry comes about mainly due to the relative movement of the Ti atoms to the O_6 octahedra that are placed at each lattice point. This relative displacement induces an electric polarization moment, since the crystal structure is non-centro-symmetric in the non-cubic phases. A schematic of the relative displacement in the different phases can be seen in Fig. 6.

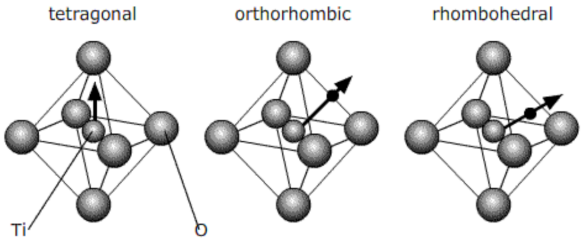

Fig. 6: Relative displacement of the Ti atom (small sphere) with respect to the O_6 octahedra using pseudo-cubic notation. From [11].

The spontaneous polarization direction with respect to the original cubic structure are $\langle 001 \rangle$ (tetragonal), $\langle 110 \rangle$ (orthorhombic), $\langle 111 \rangle$ (rhombohedral). The phase transitions occur at $120°\text{C}$, $5°\text{C}$ and $-90°\text{C}$, respectively (see Fig. 7).

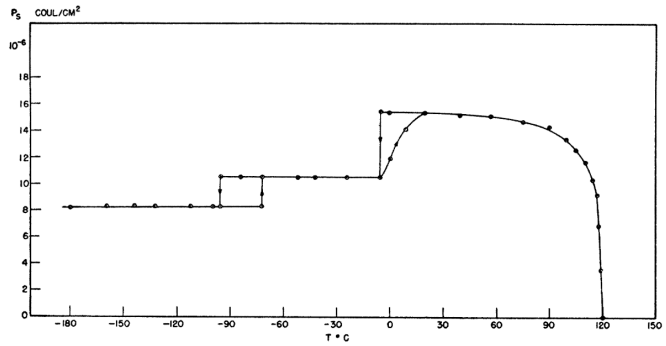

Fig. 7: Barium titanate, Spontaneous polarization P_S as a function of temperature. From [12].

Investigated Samples

For this report, we investigate the ferromagnetic behaviour of a Magnetite (Fe_3O_4) single crystal and the ferroelectric behaviour of a $BaTiO_3$-$BiFeO_3$ multilayer stack. The Magnetite sample is shaped like a prism with total volume $V_{Fe_3O_4} = 2.13 \pm 0.06$ cm^{-3} as calculated. This needs to be used later for normalization purposes. Ferroelectric measurements were performed on a $PbZr_{1-x}Ti_xO_3$ (PZT) thin film and a multi layer sample consisting of $BeFeO_3$ - $BaTiO_3$ thin films with a total thickness of $\sim$ 300nm. A schematic of the multi layer sample is shown in Fig. 8 below. Platinum point contacts (not shown) are sputtered onto the sample for measuring the polarization switching under an applied potential difference.

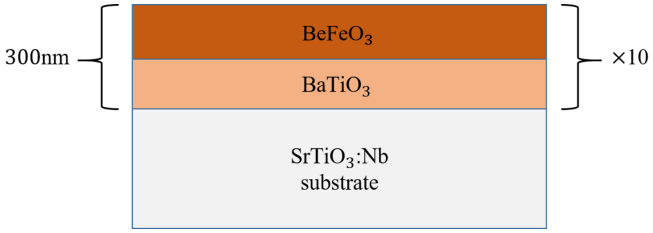

Fig. 8: Sample Schematic for ferroelectric analysis.

V. Results and Discussion

Magnetite Hysteresis loops

The hysteresis curves for two different temperatures are shown in Fig. 9. For normalization purposes, the measured magnetic moment needed to be compared to the sample volume. The two different Magnetization scaling factors on the graphs are obtained by [16]

$$M[emu/cm^3] = \frac{M[emu]}{V_{Fe_3O_4}[cm^3]} \tag{28}$$

$$M[\mu_B/f.u.] = \frac{a^3}{8} \frac{M[emu/cm^3]}{9.274 \times 10^{-21} emu/\mu_B} \tag{29}$$

where a is the cubic lattice distance. For magnetite, a is known to be $a = 8.396$ Å[13].

The saturation magnetization M_S can be seen to increase as the temperature is decreased as suggested by the Curie-Weiss law. The physical insight behind this trend is that the domain magnetization directions are statistically distributed. Random

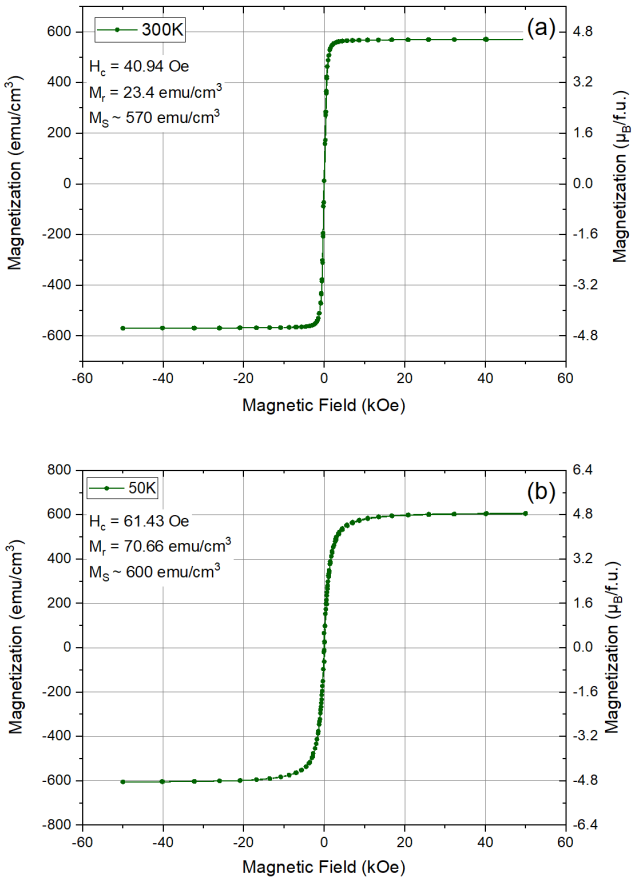

Fig. 9: Hysteresis curves for Magnetite at 300K (above) and 50K (below).

thermal fluctuations are the biggest opposing force to complete alignment of all domain magnetization vectors. Accordingly, the saturation magnetization decreses as the temperature is increased. Important to note is also the shape of the two curves. Both have quite a low remnant magnetization value M_r and coercive field H_c. Magnetite can hence be classified as being a soft magnetic material. In the ionic model, the magnetic moments of the A (Fe^{2+}) and B (Fe^{2+}/Fe^{3+}) sites are 5 and 4 μ_B, respectively. At 0K, the net moment is thus $4\mu_B/f.u.$. Measurements by Weiss and Forrer in 1929 [15] determined the saturation magnetization to be $4.07\mu_B/f.u.$. Our measured value at 50K however, is already much larger, about $4.8\mu_B/f.u.$ which is most likely due to an inaccurate measurement of the sample volume. The coercivity values are quite typical for magnetite. According to [14], typical values range between 2.4 and 20 kA/m, which corresponds to 30 and 2800 Oe, respectively.

Temperature dependence and Verwey transition

Subsequently, the magnetization in two different modes ZF (zero field) and ZFC (zero field cooled) was recorded for a temperature range between 5 and 300 K (see Fig. 10). From high temperatures, the magnetization is seen to increase until at around 120 K (the Verwey temperature), a sudden phase transition occurs which leaves the magnetization at a lower

(approximately constant) value. At the Verwey temperature, the material conductivity changes from being a metal to an insulator. This marked the first metal-insulator transition ever observed and sparked a multitude of scientific investigations until today and stimulated a still unresolved debate over a complete description of the Verwey transition. The classical description first given by Verwey in 1939 [17] is that of ionic charge ordering in the crystal. A theory, for which necessary evidence could not be found since [18]. Nonetheless, the simple model is still popular. We will shortly discuss the classical model given by Verwey and describe it's shortcomings. The model assumes that above T_V, Fe^{3+} and Fe^{2+} are dynamically disordered in the lattice. Charge movement is possible by dynamic transformations of the Fe^{2+} to Fe^{3+} ions and explains the conductivity above T_V. Below T_V, Verwey proposed that a phase transition into a highly ordered configuration of Fe^{3+} and Fe^{2+} takes place that reduces the conductivity by localizing the electrons. Structurally, the transition corresponds to a phase transition from cubic to orthorhombic phase, where the ions occupy alternately the (001) planes and form homovalent ion channels along the $[1\,1\,0]$ and $[\bar{1}\,1\,0]$ directions [18]. The magnetic moment direction is thus in the $[0\,0\,1]$ direction below T_V and along $[1\,1\,1]$ above. Neutron diffraction experiments first apparently confirmed the ionic ordering in 1958 [19], but later it was discovered that the observed reflection was, in reality, not authentic. Other experimentalists even found evidence that would directly contradict the Verwey model. Another quantity that is influenced by the phase transition at the Verwey temperature apart from the already mentioned conductivity is the heat capacity, which experiences an anomaly.

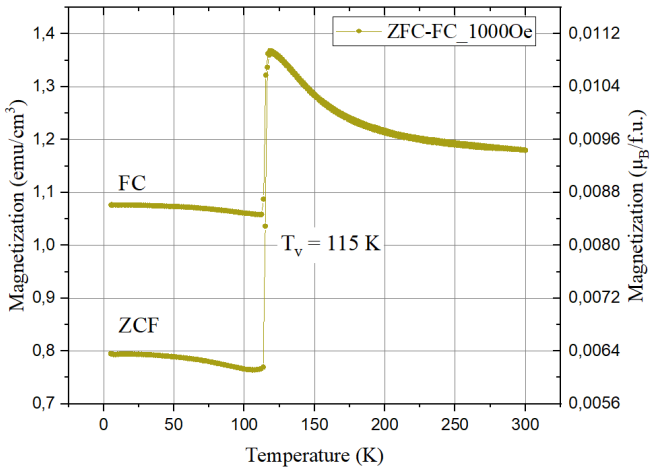

Fig. 10: Temperature dependence of magnetization in Magnetite. The Verwey transition can be observed as a peak in both measuring modes around 115 K.

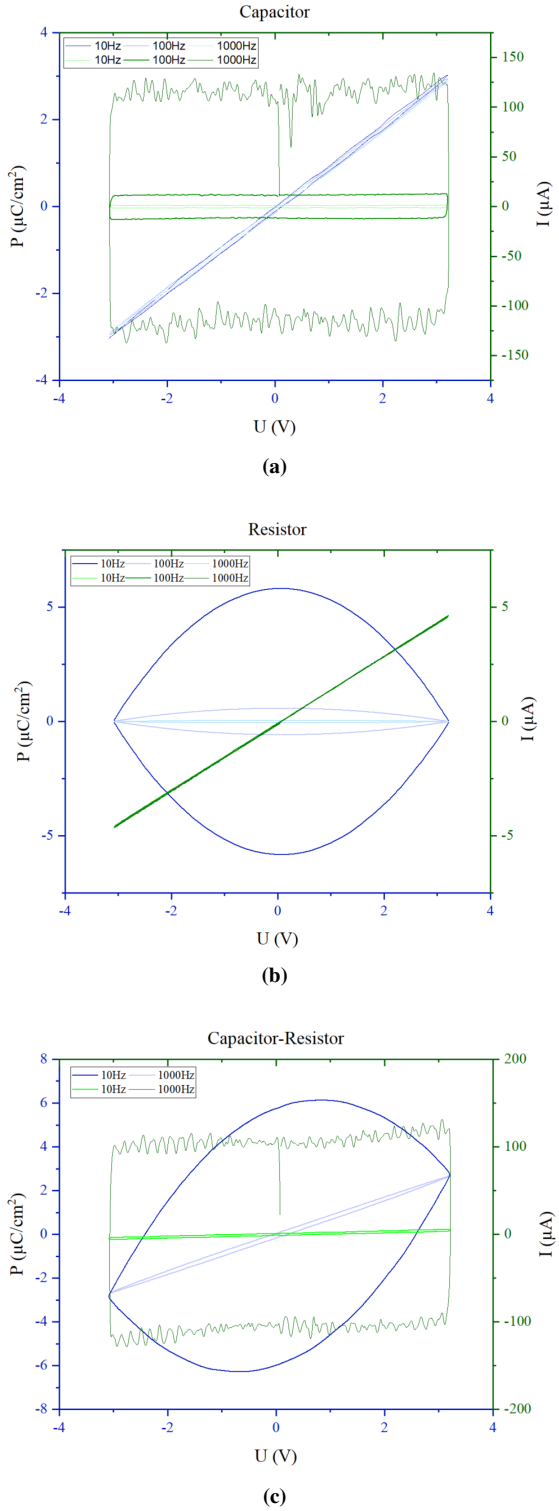

Fig. 11: The P-U curves (blue) alongside the I-U curves (green) for the three circuit elements/configurations. In (c), the resistor and capacitor are connected in parallel.

Ferroelectric Measurement of Circuit Elements

Alongside measuring the hysteresis curves for the ferroelectric samples, the electric response of three circuit setups was investigated. The plots are shown in Fig. 11 and are discussed below:

1) Since for a capacitor, $I = C\frac{dU}{dt}$, it follows from eqn. 27 that the polarization in a capacitor is linearly dependant on the voltage/electric field across it with an invariance under f variation. Conversely, since U has constant, frequency-dependant slope at all times (only differing by a sign and a discontinuity at the extrema points),

the $I(U)$ curves are just (f dependant) constants with a change of sign at the domain edges.

2) As expected from Ohm's law $I = U/R$, if the circuit contains a single resistor, the current depends linearly on the voltage and is invariant to an f variation. As $\mathbf{P}$ is calculated using $\mathbf{P} = \int Idt/A$, the resulting function $\mathbf{P}(U)$ will be a double parabola. Indeed, since $U(t)$ follows a triangular pulse dependence, the relation between dt and U at all times will be linear, where the slope is dependant on the frequency. Thus the $P(U)$ curves are double parabolas, with f dependance.
3) For the circuit setup, in which resistor and capacitor are connected in parallel, the $P(U)$ curve lifts from the horizontal line and the opening of the parabolic shape is increased with f due to the resistive component in the circuit. The point of this discussion is to show that pseudo-hysteresis loops, such as those created by the two component circuit are fairly common and can easily be mistaken as (real) ferroelectric hysteresis loops, in which polarization switching occurs.

This discussion is mainly based on [20].

PZT layer

Hysteresis curves for the single layer PZT are shown in Fig. 12 for three frequencies. An additional measurement at $f = 1000Hz$ with hysteresis amplitude of $5V$ is shown. Fig. 13 shows the I-U curves for the sample. The peaks correspond to the switching currents in the sample and are measured at the coercive voltages of about 1.33V (averaged over all results). Non-zero current values at voltages other than the coercive voltage reflect leakage currents. Upon comparison with the capacitor-resistor circuit model (Fig. 11c), a major qualitative difference becomes quite obvious. The effect of polarization switching cannot be observed in the model. Additionally, it can be noted that the saturation polarization value P_s is apparently dependant on the electric field frequency.

Multilayer sample

In Fig. 14, the hysteresis curves are seen for several hysteresis amplitudes (colorbar), measured at $f = 1$kHz. For low amplitudes, i.e. below the coercive voltage of the multilayer material, the hysteresis curves are directly comparable to the above describes capacitor-resistor model (see also the rectangular shaped I-U curves in Fig. 15). At intermediate voltages, close to the coercive voltage, the curves become asymmetric, taking a cigar shape. When the hysteresis amplitude is much larger than the coercive voltage, curves like that shown in blue/purple emerge. For the current. switching peaks can be observed clearly, albeit asymmetrically. Physical reasons for this asymmetry are due to imprint and self-poling, discussed in detail in [20].

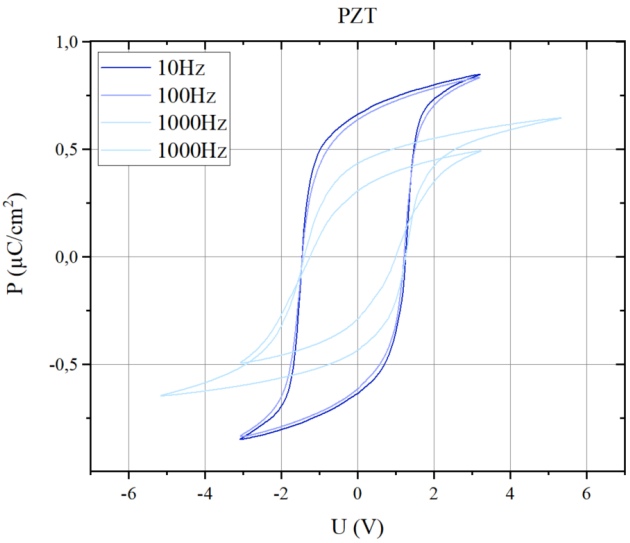

Fig. 12: PZT - P-U curves

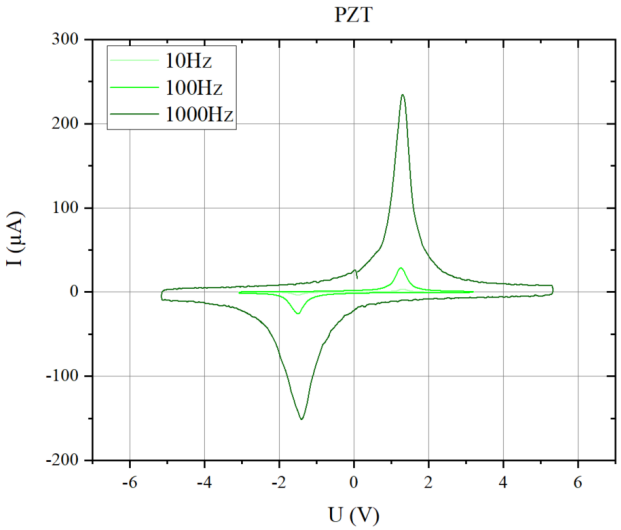

Fig. 13: PZT - I-U curves

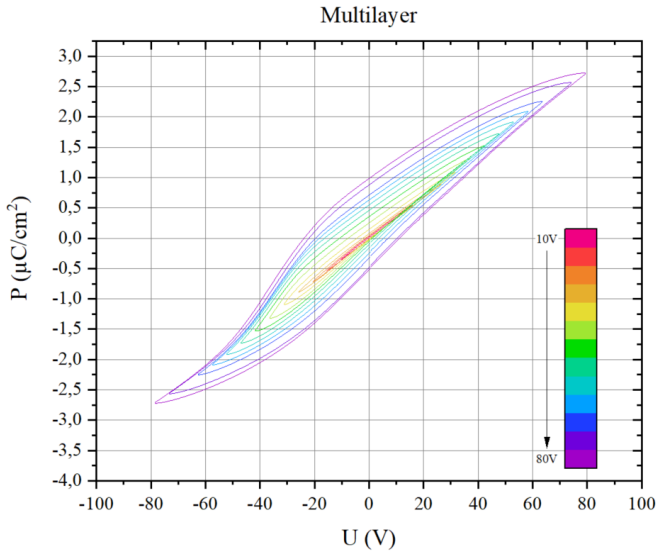

Fig. 14: Multilayer - P-U curves. The colorbar indicates the hysteresis amplitudes of the measurements in steps of 5V.

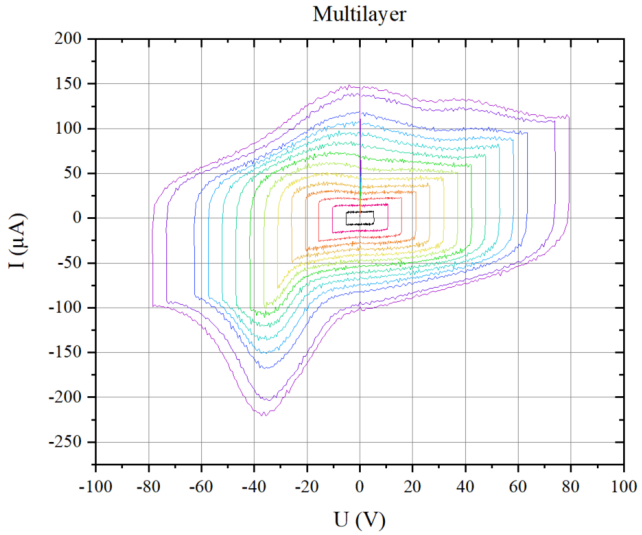

Fig. 15: Multilayer - I-U curves

REFERENCES

[1] F. Tyler B.Sc. A.Inst.P. (1931) XLIX. *The magnetization-temperature curves of iron, cobalt, and nickel*, The London, Edinburgh, and Dublin Philosophical Magazine and Journal of Science, 11:70, 596-602, DOI: 10.1080/14786443109461711

[2] P. Weiss, J. Phys. Theor. Appl. 6, 661-690 (1907) DOI: 10.1051/jphystap:019070060066100

[3] Heisenberg, W. Zur Theorie des Ferromagnetismus. Z. Physik 49, 619–636 (1928). https://doi.org/10.1007/BF01328601

[4] Spaldin, N. (2010). Interactions in ferromagnetic materials. In Magnetic Materials: Fundamentals and Applications (pp. 65-78). Cambridge: Cambridge University Press. doi:10.1017/CBO9780511781599.006

[5] Coey, J. (2010), *Magnetism and Magnetic Materials*. Cambridge: Cambridge University Press.

[6] E.S. Gorkunov, Yu.N. Dragoshansky (2000). *Interaction Between domain walls and structural defects as a background for magnetic inspection of steel structures*

[7] Louis Néel 1952 Proc. Phys. Soc. A 65 869

[8] C. G. Shull and J. Samuel Smart. Phys. Rev. 76, 1256 – Published 15 October 1949

[9] J. Valasek. Phys. Rev. 17, 475 – Published 1 April 1921

[10] Quantum Design, Vibrating Sample Magnetometer (VSM) Option User's Manual, 1096-100, Rev. B0, February 2011.

[11] DoITPoMS, University of Cambridge,[Acccessed: 12 April 2022]. https://www.doitpoms.ac.uk/tlplib/ferroelectrics/phase_changes.php#:~:text=Above%20120%C2%B0C%2C%20barium,titanate%20is%20120%C2%B0C.

[12] Walter J. Merz Phys. Rev. 76, 1221 – Published 15 October 1949

[13] R. M. Cornell and U. Schwertmann, *The iron oxides: structure, properties, reactions, occurrences and uses*. John Wiley & Sons, 2003

[14] U. Meisen and H. Kathrein, *The Influence of Particle Size, Shape and Particle Size Distribution on Properties of Magnetites for the Production of Toners*, Journal of Imaging Science and Technology 44: 508–513 (2000).

[15] Weiss P and Forrer R 1929 Ann. Phys. 12 279

[16] M. S. V. Zviagin, *Ellipsometric determination of cation disorder in magnetically ordered spinel ferrite thin films*, 2019. Leipzig University, PhD dissertation.

[17] Nature 144, 327–328 (1939). https://doi.org/10.1038/144327b0

[18] Joaqín García and Gloria Subías 2004 J.Phys.: Condens. Matter 16 R145

[19] Hamilton W C 1958 Phys. Rev. 110 1050

[20] S. Hohenberger, *Magnetoelectric Coupling in BaTiO3-BiFeO3 Multilayers: Growth Optimization and Characterization*, 2020. Leipzig University, PhD dissertation.